This article has been accepted for publication in a future issue of this journal, but has not been fully edited. Content may change prior to final publication. Citation information: DOI 10.1109/JESTPE.2018.2823904, IEEE Journal of Emerging and Selected Topics in Power Electronics

Decoupled Active and Reactive Power Predictive Control for PV Applications using a Grid-tied Quasi-Z-Source Inverter

Sarthak Jain, *Student Member*, *IEEE*, Mohammad B. Shadmand, *Member, IEEE*, and Robert S. Balog, *Senior Member*, *IEEE*

***Abstract*— This paper proposes a predictive power control algorithm that decouples active and reactive power for grid integration of photovoltaic (PV) systems using a quasi-Z-source inverter (qZSI). This is important to meet the emerging smart inverter requirements for grid interconnection. The proposed controller uses model predictive control (MPC) framework to ensure that the maximum available power is harvested from the PV array and that the active and reactive power injected into the grid is controlled to compensate reactive power required by local loads and as need to ensure stable operation of the grid at the point of common coupling (PCC). Thus, a power electronics interface (PEI) is proposed to integrate the PV array to the grid and to work as a reactive power compensator simultaneously. A robust technique is proposed to regulate the impedance network voltage and current according to the maximum operating point of PV panels and grid voltage/current requirements. The proposed controller features a simple structure suitable for practical implementation, fast dynamic response under changing sky condition, and negligible tracking error in steady state for decoupled active and reactive power control in a typical distributed generation (DG) systems. The performance of the proposed controller is verified experimentally; the grid-side power quality analysis is provided and evaluated according to IEEE-519 standard.**

***Index Terms*—Impedance source inverter, model predictive control, reactive power compensation, grid-tied inverter, PV system**

I. INTRODUCTION

Growth in the energy demand coupled with aging infrastructure and increasing concern over environmental impact is driving the development of Distributed Generation (DG) systems that support Renewable Energy Sources (RES) like solar, wind, thermoelectric, fuel cell etc. Increases in cell efficiency and reduction in total system costs, including ease of installation, has made photovoltaic energy systems not only affordable, but in some markets cheaper than energy from conventional sources [1, 2]. However, PV cells produce low, direct-current (DC) voltage as compared with the high-voltage alternating current (AC) grid and thus require power electronics for step-up, dc/ac conversion and maximum power point tracking (MPPT) for efficient operation. This generally requires multiple power converter stages to accomplish. Many of the common PV inverter topologies are two-staged with an energy buffer, such as dc-link capacitor [3]. The first stage performs MPPT, boosts the PV voltage and transfer the PV power to the energy buffer, the energy buffer is followed by second inverter stage to connect the system to the utility grid [4]. This two-staged system configuration decreases the efficiency as well as the dynamic response of the system with respect to both changes in environmental conditions and grid perturbations. In addition, the inverter is being required to provide smart-grid interface and enhanced inverter functionality. Thus, the ideal DG based power electronics interface needs a single conversion stage for high efficiency, a comprehensive and robust controller for grid interaction, and multiple modes to accomplish the PV-side and grid-side control.

Several techniques have been proposed for single stage grid connection of the PV in which the inverter performs both MPPT and inversion functions [3]. However, as these topologies are either voltage sourced or current sourced inverters, they are limited to only buck or boost operation of the PV source voltage respectively [5]. The Z-source inverter (ZSI) and quasi-Z-source inverter (qZSI) have been extensively studied for PV applications due to their capability of both buck/boost operation of DC input voltage by coupling an impedance network between power source and the inverter bridge [6-9]. ZSI/qZSI incorporates an overlap-mode switching state (commonly called *shoot through*) in which both switches of a bridge phase leg are purposely turned on which results in the boosting of the input voltage controlled by the amount of time in this overlap state (shoot through time) [10]. In comparison with traditional two stage PV energy harvesting systems which require DC/DC stage for boosting/MPPT and DC/AC stage for inversion, ZSI/qZSI can provide a more efficient, reliable, and cost-effective solution with just a single stage conversion and reduced number of active switches [5, 11]. These properties make ZSI/qZSI suitable for renewable energy sources (RES) to overcome the limitations of VSI/CSI topologies [7]. Expanding the advantages of the ZSI, the qZSI has continuous input current [11] which can eliminate problems with electro-magnetic interference (EMI), leakage/ground currents and can significantly increase PV life span and energy harvest [12-15]. In addition, the voltage across one of the two capacitors in the impedance network is lower than the other capacitor, thus supporting a lower rating capacitor which can reduce the cost, which isn't the case in ZSI [16]. Accordingly,

This publication was made possible by NPRP grant # 7-299-2-124 and NPRP-EP grant # X-033-2-007 from the Qatar National Research Fund (a member of Qatar Foundation). The statements made herein are solely the responsibility of the authors.

M. B. Shadmand is with the Department Electrical & Computer Engineering at Kansas State University, Manhattan, KS (email: mohamadshadmand@gmail.com). S. Jain and R. S. Balog are with the Department of Electrical and Computer Engineering at Texas A&M University, College Station, TX (emails: jainsarthak2091@gmail.com, robert.balog@ieee.org).

This article has been accepted for publication in a future issue of this journal, but has not been fully edited. Content may change prior to final publication. Citation information: DOI 10.1109/JESTPE.2018.2823904, IEEE Journal of Emerging and Selected Topics in Power Electronics

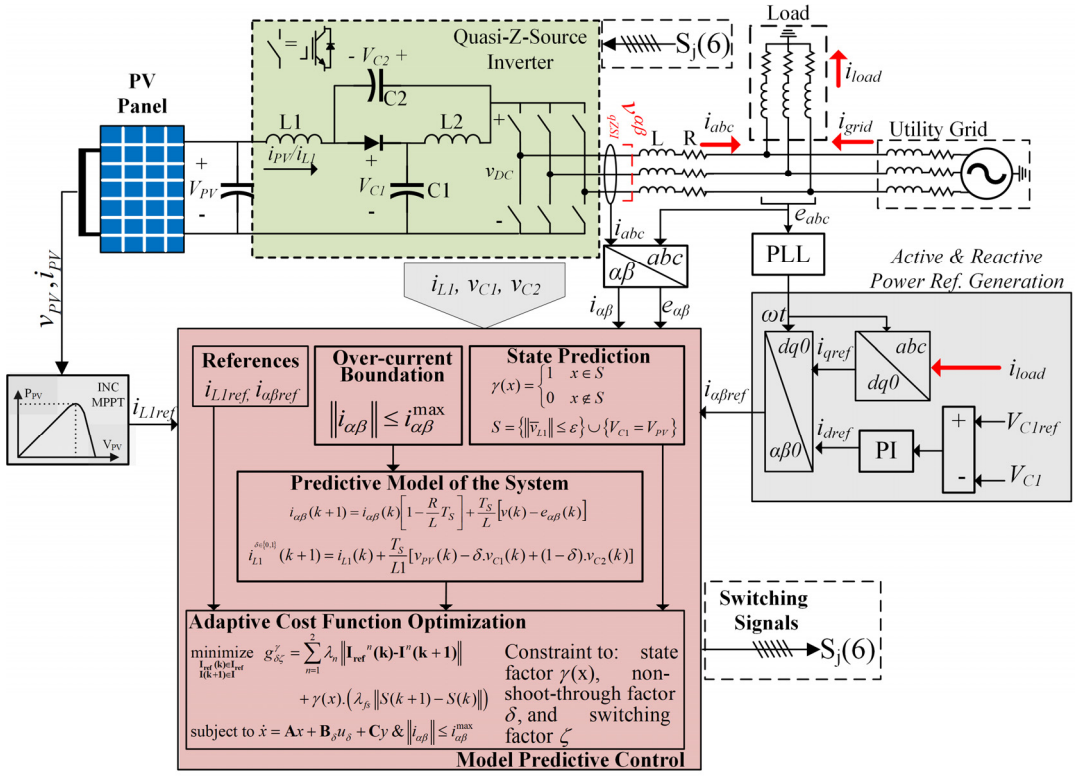

Fig. 1. Proposed power electronics interface system overview.

the voltage fed qZSI proposed in [17] is used for the proposed PV energy harvesting unit with reactive power compensation in this paper.

Due to the increasing penetration of low-power inverters into the grid distribution system, jurisdictions are developing codes and standards to maintain grid stability particularly during the transient or abnormal conditions [18, 19]. Apart from just working under MPPT conditions, RES based distributed generation (DG) systems are mandated by grid codes to have a precise and independent control over reactive power [20] and hence provide ancillary support to grid for voltage regulation at the local bus as well to maintain the overall stability of the grid [21].

The addition of the impedance network and overlap mode in the inverter of the qZSI complicates the traditional control and requires a complex modulator with multi/nested loop control system [11] to control the capacitor voltage, input inductor current along with the injected grid current [11]. Hence, for conventional control, separate control loops are required for grid integration and other mandated objectives, which could result in slow dynamic response/lower bandwidth and highly complex control design. Instead, model predictive control (MPC) is well suited to handle this multi-control objective task.

With the rapid advancements of fast and efficient digital signal processors, MPC is becoming increasingly popular for power electronics applications [22-24]. Among the two control types of MPC [25], finite set MPC has been extensively used due to its simplicity in which switching states are directly estimated and controlled without needing a modulator to create the switching signals. Also, for complex non-linear systems, MPC has been proven to be an effective solution over conventional multi/nested loop compensators which have complex structure and multi-variable tuning [11]. MPC offers various advantages like fast dynamic response, incorporation of non-linear control variables in a straightforward manner and possible implementation of conventional nested loop structure in a single loop [25-28]. Classical controller requires multi-loop variable tuning, more complex PWM modulator design and provides less modularity in the qZSI thus the advantages of the MPC controller can be seen more in qZSI application. qZSI unlike conventional VSI requires multiple objectives like input inductor current, capacitor voltage, output grid current etc. to be handled simultaneously thus require nested loop control. The presented algorithm provides a different approach to decrease the computational complexity of the control along with maintaining the various parameter control quality with minimal control effort. It eliminates the PWM modulator which is a major challenge in ZSI/qZSI system due to proper shoot-through insertion requirement [26], which requires complex logic to incorporate the shoot through state with precise timing control.

Therefore, the above-mentioned advantages motivated many researchers to focus on implementing model predictive controlled qZSI for wide range of applications. In [11], direct predictive control is used for qZSI for an off-grid system with RL load. The presented control calculated the references based on the known values of the load parameters, which is practically not the case. Also, the grid connection capability and control testing was not shown which is necessary for DG systems. The system proposed in [29] shows Z-source grid-tied PV inverter where grid synchronization is done using a simple boost pulse width modulation (PWM) strategy. In [30], MPC for direct power control is developed for off-grid systems. The system in [30] does not cover the grid integration and the system shown was for constant DC input but not for a PV source. The intermittent nature of PV can effectively change the dynamic behavior of the system. The modeling and control of qZSI for

This article has been accepted for publication in a future issue of this journal, but has not been fully edited. Content may change prior to final publication. Citation information: DOI 10.1109/JESTPE.2018.2823904, IEEE Journal of Emerging and Selected Topics in Power Electronics

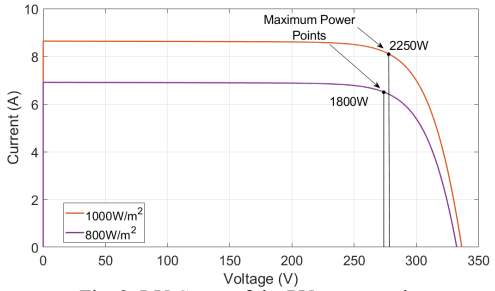

Fig. 2. I-V Curve of the PV array used.

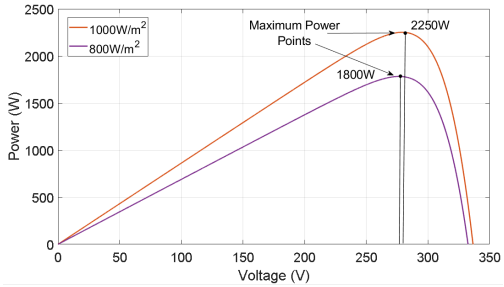

Fig. 3. P-V Curve of the PV array used

grid-connected PV system is developed in [7] by using conventional multi-loop classical control system suffering from low bandwidth and slow response. In addition, none of the above-mentioned literature discusses the problem of independent power control of qZSI for grid integration of PV systems that can simultaneously compensate the reactive power required by the grid as an ancillary service that can be provided by DG systems to main utility grid [20].

This paper proposes a control algorithm for grid-tied qZSI PV system with decoupled active and reactive power control along with energy-loss optimization per switching cycle based on MPC framework. Thus, the presented power electronics interface (PEI) can simultaneously inject the maximum harvested power to the grid and work as a reactive power compensator providing the ancillary services to the grid. The following list summarizes the contributions of the paper:

1. Active/Reactive power decoupled control with their exact reference generation for MPC.
2. Reactive power compensation at point of common coupling (PCC) using the proposed PV energy harvesting system.
3. Incorporate minimum energy controller by minimizing the switching events per cycle, thus optimizing the average switching frequency and as a result minimizing the switching losses.
4. An adaptive cost function is proposed to prioritize the active/reactive power control and power quality over the switching event minimization during dynamic changes in the system. The dynamic changes could be due to change in ambient conditions of the PV or change in the reactive power requirement at the PCC.
5. The cost function proposed in the system only uses two parameters apart from switching event minimization formulation as opposed to three parameters in conventional PEI control making it simpler to tune weight factors and reduce design complexity.

With the increased small-scale penetration of RES into the grid, the proposed PEI based-qZSI shows the promising application in highly efficient future microgrid architectures. The presented system decouples the DC bus controller from MPC using a low bandwidth PI control which performs majorly two functions, i.e., to decouple power and provide a low bandwidth, less complex DC bus controller, thereby reducing the computation burden of computing predictive values V_{C1} by solving higher order equations. This allows user to run the rest of the algorithm at higher rate thereby achieving high quality current waveforms along with low tracking error.

The decoupling and independent reference generation for active and reactive current at AC side allows more robust and modular control in context of the grid codes needs to be followed any PEI interfaced with the grid. The active/reactive power can be easily modified based on low voltage ride through (LVRT) [20] conditions like grid voltage support, load reactive power compensation, etc.

II. System Modeling

Fig. 1 shows the complete power stage with an overview of the control system adopted in this paper. Power stage includes PV array connected to qZSI with an input capacitor to stabilize the input voltage. PV module Suntech STP250-20/Wd is used to create a PV array by connecting 9 panels in series for the experiments in this paper. The I-V and P-V characteristic curves of the array shown in Fig. 2 and Fig. 3 respectively for solar irradiance levels of 1000 W/m^2 and 800 W/m^2. Then, the qZSI is tied to 3-phase grid at PCC through a first order R-L filter. The PCC is feeding some passive load demanding both active and reactive power. The three-phase grid is assumed to have impedance to test the system model for more practical and accurate scenario. The control system shown can be divided into two parts for easier understanding, named, *reference generation* based on the active and reactive power to be supplied by qZSI and *predictive control* to achieve the referenced parameters. The active power reference to be supplied by the qZSI to the PCC is generated through MPPT algorithm and reactive power reference can be generated through various ways. Reactive power demand of the system can be catered based on the load reactive power demand, which is adopted in this paper or through droop control/low-voltage ride through strategies proposed in various literature [20]. The algorithm proposed in the system can be adapted for any of the above-mentioned reactive power injection strategies based on the needs. The following sub-sections explain the modeling of the qZSI and its dynamic behavior for devising the discrete equations for MPC.

A. Quasi-Z-Source Inverter Modeling

Fig. 1 shows the PV sourced qZSI with predictive control of active and reactive power in decoupled manner. Fig. 4 shows qZSI equivalent circuit during active and shoot through state based on δ, where δ represents active state and shoot through state when its value is 1 and 0 respectively. The qZSI is analyzed in both active states and shoot through states separately to develop system equations which are required for designing MPC framework. The full switching period of the qZSI bridge is considered to be T ($T = T_1 + T_o$), active state

This article has been accepted for publication in a future issue of this journal, but has not been fully edited. Content may change prior to final publication. Citation information: DOI 10.1109/JESTPE.2018.2823904, IEEE Journal of Emerging and Selected Topics in Power Electronics

time to be T_1, shoot through state time to be T_o and shoot through duty ratio D as T_o/T. From Fig. 1 and Fig. 4, state space model can be determined as (1), (2) and (3):

$$\begin{bmatrix} \dot{i}_{l1} \\ \dot{i}_{\alpha} \\ \dot{i}_{\beta} \end{bmatrix} = \begin{bmatrix} 0 & 0 & 0 \\ 0 & \frac{-R}{L} & 0 \\ 0 & 0 & \frac{-R}{L} \end{bmatrix} \begin{bmatrix} i_{L1} \\ i_{\alpha} \\ i_{\beta} \end{bmatrix} + \begin{bmatrix} \frac{-1}{L1} & 0 & 0 \\ 0 & \frac{-1}{L} & 0 \\ 0 & 0 & \frac{-1}{L} \end{bmatrix} \begin{bmatrix} v_{C1} \\ e_{\alpha} \\ e_{\beta} \end{bmatrix} + \begin{bmatrix} \frac{1}{L1} & 0 & 0 \\ 0 & \frac{1}{L} & 0 \\ 0 & 0 & \frac{1}{L} \end{bmatrix} \begin{bmatrix} v_{PV} \\ v^{\alpha}_{qZSI} \\ v^{\beta}_{qZSI} \end{bmatrix} \quad (1)$$

$$\begin{bmatrix} \dot{i}_{l1} \\ \dot{i}_{\alpha} \\ \dot{i}_{\beta} \end{bmatrix} = \begin{bmatrix} 0 & 0 & 0 \\ 0 & \frac{-R}{L} & 0 \\ 0 & 0 & \frac{-R}{L} \end{bmatrix} \begin{bmatrix} i_{L1} \\ i_{\alpha} \\ i_{\beta} \end{bmatrix} + \begin{bmatrix} \frac{1}{L1} & 0 & 0 \\ 0 & \frac{-1}{L} & 0 \\ 0 & 0 & \frac{-1}{L} \end{bmatrix} \begin{bmatrix} v_{C2} \\ e_{\alpha} \\ e_{\beta} \end{bmatrix} + \begin{bmatrix} \frac{1}{L1} & 0 & 0 \\ 0 & \frac{1}{L} & 0 \\ 0 & 0 & \frac{1}{L} \end{bmatrix} \begin{bmatrix} v_{PV} \\ v^{\alpha}_{qZSI} \\ v^{\beta}_{qZSI} \end{bmatrix} \quad (2)$$

$$\overline{v}_{L1} = \frac{T_o(V_{C2} + V_{PV}) + T_1(V_{PV} - V_{C1})}{T} \quad (3)$$

The equations (1)-(2) are written in standard form as, $\dot{x} = \mathbf{A}x + \mathbf{B}_{\delta}u_{\delta} + \mathbf{C}y$. The parameters for active state ($\delta=1$) and shoot-through state ($\delta=0$) as A, B_0, B_1 and C where B_0 is for shoot-through states and B_1 for active states matrices are as follows:

$$\mathbf{A} = \begin{bmatrix} 0 & 0 & 0 \\ 0 & \frac{-R}{L} & 0 \\ 0 & 0 & \frac{-R}{L} \end{bmatrix} \qquad \mathbf{B}_0 = \begin{bmatrix} \frac{-1}{L1} & 0 & 0 \\ 0 & \frac{-1}{L} & 0 \\ 0 & 0 & \frac{-1}{L} \end{bmatrix}$$

$$\mathbf{B}_1 = \begin{bmatrix} \frac{1}{L1} & 0 & 0 \\ 0 & \frac{1}{L} & 0 \\ 0 & 0 & \frac{1}{L} \end{bmatrix} \qquad \mathbf{C} = \begin{bmatrix} \frac{1}{L1} & 0 & 0 \\ 0 & \frac{1}{L} & 0 \\ 0 & 0 & \frac{1}{L} \end{bmatrix}$$

where the state vector is $x = \begin{bmatrix} i_{L1} & i_{\alpha} & i_{\beta} \end{bmatrix}^T$, the input vector is $u_0 = \begin{bmatrix} v_{C2} & e_{\alpha} & e_{\beta} \end{bmatrix}^T$ and $u_1 = \begin{bmatrix} v_{C1} & e_{\alpha} & e_{\beta} \end{bmatrix}^T$ for shoot through and active state respectively. Control output vector is $y = \begin{bmatrix} v_{PV} & v^{\alpha}_{qZSI} & v^{\beta}_{qZSI} \end{bmatrix}^T$ where v_{PV} is the instantaneous PV voltage, v^{α}_{qZSI} and v^{β}_{qZSI} as the instantaneous bridge output voltage vector in α and β frame. Using state-space averaging, inductor voltage in (1)-(2) can be simplified over the complete switching cycle T in terms of D (shoot through duty ratio) and (1-D) as active state duty ratio which results in average voltage given by (3). The average inductor (L1) voltage (3) will be zero in case of steady state operation and this technique will be used later to detect the state (transient or steady state) of the system and develop an adaptive MPC cost function to prioritize the control and provide fast dynamic performance. It is worth mentioning that, the proposed method only uses L1 voltage for the state (transient or steady state) detection to reduce the computation and redundancy; the detail of this state detection technique is explained in section III. D.

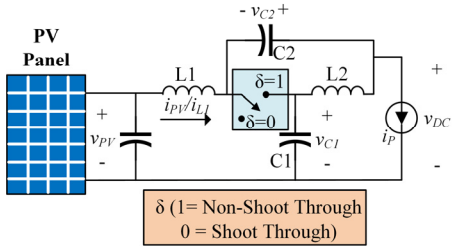

Fig. 4. qZSI equivalent circuit in Non-Shoot through (δ=1) and Shoot through state (δ=0)

B. Filter-grid Interface Modeling

In the proposed PEI, qZSI is connected to the grid through L filter with equivalent loss resistance of R. This paper doesn't deal with the filter dynamics and its effects on the system, thus a simple R-L filter is chosen for reduced complexity, although, the system can be extended to the higher order filters like LCL or LLCL with proper modifications in the presented control and careful design of the filter [31-34]. The behavior of the system at the inverter-grid junction (PCC) is described as:

$$v^{abc}_{qZSI} = Ri_{abc} + L\frac{di_{abc}}{dt} + e_{abc} \quad (4)$$

Here, v^{abc}_{qZSI} is the present output voltage vector of qZSI, i_{abc} is the injected current into system through R-L filter and e_{abc} is the instantaneous PCC voltage. The grid voltage has been measured at the PCC. All the three phase vectors can be represented as $\boldsymbol{\xi}_{\mathbf{abc}} = \begin{bmatrix} \xi_a & \xi_b & \xi_c \end{bmatrix}^T$. The system is further analyzed in $\alpha\beta$ complex frame for MPC framework (Section III.B) to reduce the number of equations from 3 to 1 complex equation. The time domain system model in $\alpha\beta$ frame can be transformed using $\boldsymbol{\xi}_{\boldsymbol{\alpha\beta}} = \mathbf{K}\boldsymbol{\xi}_{\mathbf{abc}}$, where $\mathbf{K}$ is Clarke's transformation matrix.

$$v^{\alpha\beta}_{qZSI} = Ri_{\alpha\beta} + L\frac{di_{\alpha\beta}}{dt} + e_{\alpha\beta} \quad (5)$$

Here, each quantity with $\alpha\beta$ is taken in complex form as $x_{\alpha\beta} = x_{\alpha} + jx_{\beta}$.

III. Control Design with Predictive Model

The control design for the system shown in Fig. 1 can be divided into six parts: (A) reference generation for MPC, (B) predictive model of the qZSI and its grid interface, (C) optimal control effort, (D) system state determination for adaptive cost function implementation, (E) cost function formulation and minimization, and (F) Lyapunov stability analysis of the

This article has been accepted for publication in a future issue of this journal, but has not been fully edited. Content may change prior to final publication. Citation information: DOI 10.1109/JESTPE.2018.2823904, IEEE Journal of Emerging and Selected Topics in Power Electronics

system. All these parts will be explained separately in detail in the following sub-sections.

A. Reference Generation for MPC

Overview block diagram of reference generation is shown in Fig. 1. As discussed in introduction (Section. I), qZSI control requires multiple quantities to be controlled simultaneously. In general, for a qZSI, v_{C1}, i_{L1} and i_{abc} is controlled [11], however, the proposed algorithm does not include V_{C1} in the cost function thus providing a simpler multi-objective predictive controller and easier weight function tuning. A PI controller is used for the regulation of $V_{C1.}$ DC bus voltage reference tells the PI controller about the amount of current need to be extracted from the bus which converts into the real power on the AC side. Here, decoupled active/reactive power controller is proposed which requires the independent control of both the power or their power components i.e. i_d and i_q. MPC is used to achieve the reference value of the currents on the AC side and the DC side only. PI is used to provide the $i_{d,ref}$ as explained and is combined with the $i_{q,ref}$ to make the total AC currents needs to be injected by the qZSI on the AC side. This way a decoupled control is achieved which is not possible if we include the V_{C1} in the MPC itself as it will try to achieve the different AC current form and won't have any i_q component. Thus, using PI module allows us to realize a decoupled power control, less complex MPC while maintaining high quality current controller, easy tuning of the system and less computation time for the system.

The reference for V_{C1} is considered to be 600V [35, 36] which is more than the double of the considered utility grid having 208 V_{RMS}(L-L) to transfer active power easily [37] and also to compensate high reactive power demand. The reference value for V_{C1} can be altered based on the system requirements for active and reactive power.

The Conventional Incremental and Conductance (INC) [38] algorithm is used to generate PV current reference, which is the $i_{L1,ref}$ in steady state due to charge balance on the input capacitor shown in Fig. 1. An input capacitor is used with PV to eliminate the ripple current from PV, which can eliminate the voltage ripple and provide voltage stability at the input and does not change the DC component of PV current, $i_{PV,ref}$ from $i_{L1ref,}$. In addition, the i_q part is presented as general parameter and left on reader to decide its source as it can be based on different goals. For example, in current paper, i_q has been generated to make the grid work at unity power factor thus compensating for all the reactive power required at the PCC by local load. User can extend this methodology and use latest grid codes, LVRT requirements etc. to find the reactive power (i_q) reference needs to be injected into the grid. The i_{qref} (reactive power component) is generated based on the reactive power requirement of the grid which can be either estimated based on the connected load by sensing the load reactive current component (i_{qload}) as adopted in this paper and shown in Fig. 1 or by providing the Q_{ref} through different ways mentioned in the *Introduction* section of this paper. After finding i_d and i_q, they are converted into $\alpha\beta$ stationary frame using PLL. In ideal system, we can directly convert the i_{L1ref} to the output i_{abcref} using output voltage as the losses are considered zero and grid voltage is stiff. But, here the PI module is used which can cater for the losses in the whole system making it more practical and robust as compared with the previous presented work in which the references are generated assuming zero losses in conversion. The zero-loss consideration can also lead to system instability due to power mismatching at input/output ports. The two references, i_{L1ref} and $i_{\alpha\beta ref}$ are then fed to the MPC block for further processing and switching signal generation. The MPC block is executed at fixed sampling time of T_s and estimates the appropriate switching vector for $k+N$ sampling interval, where in this paper one step prediction ($N=1$) is used. Thus, the whole control is analyzed as two independent systems like in the two-stage grid connected system with DC side MPPT being the first stage and inverter side doing grid synchronizations being second, although, here both are used to control the single inverter bridge unit.

B. Predictive Model of the System

Predictive model of the system is determined by discretizing continuous time domain equations explained in Section II. Sampling frequency is chosen high enough to have an accurate prediction while meeting the hardware processor capability to execute the control loop efficiently for experimental implementation. With sufficiently high sampling frequency, the system can be approximated using forward Euler method as explained in [39]. This sub-section develops the predictive model equations for the qZSI-filter-grid interface and the impedance network inductor (L1) current at PV side of qZSI.

The $i_{\alpha\beta}$ current predictive model is developed by considering qZSI output voltage vector as $v_{qZSI}^{\alpha\beta}$ which is interfaced with grid having voltage of $e_{\alpha\beta}$ at PCC through R-L filter. The continuous time system mode given by (5) is discretized and used to predict the $i_{\alpha\beta}$ current using forward Euler method as:

$$i_{\alpha\beta}(k+1) = i_{\alpha\beta}(k)\left[1-\frac{R}{L}T_S\right] + \frac{T_S}{L}\left(v_{qZSI}^{\alpha\beta}(k) - e_{\alpha\beta}(k)\right) \quad (6)$$

where, k is the present sampling instant and k+1 is the predicted sample one step ahead in horizon of time. All the parameters are defined in $\alpha\beta$ complex frame of reference converting three equations to *one complex equation*.

To predict the future values of inductor current (i_{L1}), both shoot-through and active state model equations given by (1) and (2) are used. Using the voltage-current relationship for an inductor and discretizing it using forward Euler method, with mathematical re-arrangements, the inductor ($L1$) predicted current can be determined by:

$$i_{L1}^{\delta\in\{0,1\}}(k+1) = i_{L1}(k) + \frac{T_S}{L1}\left[v_{PV}(k) - \delta.v_{C1}(k) + (1-\delta).v_{C2}(k)\right] \quad (7)$$

where $i_{L1}(k+1)$ is the predicted value of inductor current and δ is active state indicator as described in Section II.A.

C. Optimal Control Effort: Minimizing the Energy-loss per Switching Event

Switching frequency is a critical parameter that influences the switching losses of the converter. IGBTs are extensively used for grid-tied inverters applications due to their high voltage rating and low conduction losses as compared to the same rated Si-MOSFETs. However, IGBT has switching frequency limitation and generally, they are restricted to approximately maximum value of 20~30 kHz. Thus, an effective controller should minimize the switching frequency while maintaining the quality of power injection to the system.

This article has been accepted for publication in a future issue of this journal, but has not been fully edited. Content may change prior to final publication. Citation information: DOI 10.1109/JESTPE.2018.2823904, IEEE Journal of Emerging and Selected Topics in Power Electronics

The proposed algorithm accounts for extra term in cost function, which minimizes the switching changes per switching event thus achieving a minimum energy controller. The switch state change from instant k to k+1 is formulated as:

$$\Delta S(k+1) = S(k+1) - S(k) \tag{8}$$

where S(k) and S(k+1) are the current switching vector and the switching vector to be applied to qZSI at instant (k+1). To achieve a minimum energy controller, the following penalty function is added to the MPC cost function:

$$g_{fs} = \lambda_{fs} \left\| \Delta S(k+1) \right\| \tag{9}$$

By minimizing (9) with weight factor of λ_{fs}, the average energy loss per switching cycle will be reduced.

D. System State Determination

The determinations of the system state are done based on the estimated input inductor (L1) voltage by MPC, the average voltage value of the inductor is computed for every switching cycle (T) based on (3). The MPC algorithm is running at a constant sampling frequency of f_s generating a switching vector every T_s second. The proposed algorithm will count the number of sample (T_s) time (N_1) for which the output vector is in shoot-through (S_9) and number of sample time (N_2) output vector is in active (non-shoot through) state ($S_j \mid j \in [1,8], j \in \mathbb{Z}$) before going into shoot through again. There is a possibility of the qZSI to operate without going in shoot through state, which is only possible when v_{PV} is equal to v_{C1} in (3). The time periods used in (3) can be estimated using the following integers:

$$T_o = N_1 T_S, T_1 = N_2 T_S \Rightarrow T = (N_1 + N_2) T_S \tag{10}$$

There are two possible scenarios of the operation of the qZSI:

1) If N1≠0, meaning the qZSI is boosting the input voltage PV by employing shoot-through state during its operation. In this scenario, the average voltage of the inductor given by equation (3) will be used to determine the state of the system. Time periods T_o, T_1 and T calculated by using equation (10) will be used to balance the inductor volt-sec which should balance in steady state and should be equal to a small value of voltage drop across its ESR only. If volt-sec doesn't balance, that means system is in transient mode and changing the inductor current.
2) If N1=0, qZSI is not boosting the input PV voltage and thus, is not employing shoot through states during its operation. During this case, the capacitor C1 voltage will be equal to the input PV voltage.

TABLE I: SWITCHING TABLE

Switching State	S_1	S_2	S_3	S_4	S_5	S_6	Voltage Magnitude	Angle
000	0	1	0	1	0	1	0	0
100	1	0	0	1	0	1	$\frac{2}{3}V_{DC}$	0
110	1	0	1	0	0	1	$\frac{2}{3}V_{DC}$	$\frac{\pi}{3}$
010	0	1	1	0	0	1	$\frac{2}{3}V_{DC}$	$\frac{2\pi}{3}$
011	0	1	1	0	1	0	$\frac{2}{3}V_{DC}$	π
001	0	1	0	1	1	0	$\frac{2}{3}V_{DC}$	$\frac{4\pi}{3}$
101	1	0	0	1	1	0	$\frac{2}{3}V_{DC}$	$\frac{5\pi}{3}$
111	1	0	1	0	1	0	0	0
S9 (Shoot Through)	1	1	1	1	1	1	0	0

Statement (11) estimates system state factor $\gamma(x)$ by returning 1 (steady state) if the equation is true, 0 otherwise (transient):

$$\gamma(x) = \begin{cases} 1 & x \in S \\ 0 & x \notin S \end{cases}$$
$$S = \left\{ \left\| \bar{v}_{L1} \right\| \le \varepsilon \right\} \cup \left\{ V_{C1} = V_{PV} \right\} \tag{11}$$

$\bar{v}_{L1}$ is the average value of inductor voltage from (3) and V_{C1} and V_{PV} are the average values of capacitor C1 voltage and input PV voltage over one switching cycle. ε is the error tolerance for $\bar{v}_{L1}$ as in practical cases, there would be a small DC component of voltage across the inductor due to its ESR. This error tolerance is an important property, as $\bar{v}_{L1}$ will never be zero in any practical case.

The final task of the proposed controller is the over-current protection. The proposed MPC cost function is subject to the constraint given by (12) which bound the output current within a predefined limit:

$$\left\| i_{\alpha\beta} \right\| \le i_{\alpha\beta}^{\max} \quad \text{where } i_{\alpha\beta}^{\max} \in \mathbb{R}^+ \tag{12}$$

The inverter current is constrained by this bound in the optimization of the cost function. This also enforces inverter over-current protection and avoids large inrush current during grid faults and supports LVRT [40]. The bound value $i_{\alpha\beta}^{\max}$ can be set around 90% of the rating of the semiconductor devices used giving a proper headroom to compensate for the various parametric variations in the devices due to heating, ageing etc.

E. Cost Function Computation

In this paper, the cost function computation and minimization is done based on the current state of the system, i.e. transient or steady state. To provide maximum dynamic response while maintaining the lower switching frequency, the system ignores the switching loss optimization during transients to achieve the reference values faster after which the control is switched to work optimally reducing switching effort and energy-loss per switching event. The general form of the cost function is given by (13) with its matrices in Table. II.

$$\begin{aligned} \underset{\substack{\mathbf{I_{ref}(k)} \in \mathbf{I_{ref}} \\ \mathbf{I(k+1)} \in \mathbf{I}}}{\text{minimize}} \quad & g_{\delta\zeta}^{\gamma} = \sum_{n=1}^{2} \lambda_n \left\| \mathbf{I_{ref}}^n \mathbf{(k)} - \mathbf{I}^n \mathbf{(k+1)} \right\| \\ & + \gamma(x).\left(\lambda_{fs} \left\| S(k+1) - S(k) \right\| \right) \\ \text{subject to } & \dot{x} = \mathbf{A}x + \mathbf{B}_\delta u_\delta + \mathbf{C}y \\ & \left\| i_{\alpha\beta} \right\| \le i_{\alpha\beta}^{\max} \\ & \gamma(x) \in \{0,1\}, \delta \in [0,1], \zeta \in [1,9] \ \ \& \ \delta, \zeta \in \mathbb{Z} \end{aligned} \tag{13}$$

Here, the cost function is divided into two parts: major system control objectives and auxiliary minimization of energy loss per switching event. The cost function is minimized based on the system equations developed earlier. In addition, the output current protection is considered while minimizing the cost

This article has been accepted for publication in a future issue of this journal, but has not been fully edited. Content may change prior to final publication. Citation information: DOI 10.1109/JESTPE.2018.2823904, IEEE Journal of Emerging and Selected Topics in Power Electronics

Algorithm 1: Proposed MPC Algorithm

1: *function* PredictiveControl() *sampling* at T_s
Input: $i_{L1}(k)$, $v_{C1}(k)$, $v_{C2}(k)$, $i_{abc,ref}(k)$, $i_{abc}(k)$, $e_{abc}(k)$, $v_{PV}(k)$
Initialization: $N_1, N_2 = 0$
2: *Conversion* from *abc* to *αβ* frame
$x_{\alpha\beta,} = \mathbf{K}x_{abc,} \,|\, x \in \{e_{abc}, i_{abc}, i_{abc,ref}\}$
3: *Loop-1:* State Prediction
Count N_1, number of times output of MPC is shoot-through consecutively.
Count N_2, number of times output of MPC is non-shoot through state between two shoot-through states.
$\gamma(x) \Leftarrow$ Compute from (3), (10), and (11)
4: *Loop-2:* Predictive Control & Cost function Computation
for $i = 0,\ldots,8$:
grid prediction model:
$i_{\alpha\beta}(k+1)_{(i)} \Leftarrow$ Compute from (6) $\forall$ S_j
subject to ζ
qZSI Predictive model:
$i_{L1}(k+1)_{(i)} \Leftarrow$ Compute from (7) $\forall$ S_j
subject to δ, ζ
Compute $g^{\gamma}_{\delta\zeta}(i) = g_{\delta\zeta}(i) + g^{\gamma}_{fs}(i)$ **from** (13)
subject to $\dot{x} = \mathbf{A}x + \mathbf{B}_{\delta}u_{\delta} + \mathbf{C}y$
$\left\| i_{\alpha\beta} \right\| \le i^{\max}_{\alpha\beta}$
with constraint of *state factor (γ(x)), non-shoot through indicator (δ), and switching factor (ζ).*
end for
5: *Loop-3:* Cost function minimization
$g_{\min} \Leftarrow \infty, i_{\min} \Leftarrow 0$
for i=0,…,8
if $g^{\gamma}_{\delta\zeta}(i) \le g_{\min,}$ *then*
$g_{\min} \Leftarrow g^{\gamma}_{\delta\zeta}(i), i_{\min} \Leftarrow i$
end if
end for
6: *Return switching state*
Return S_i (switching state corresponding to ***i***, generating minimum error)
end function

functions. The cost function is adaptive in a sense that it is constrained by $\gamma(x), \delta$, and ζ.

The proposed predictive controller Algorithm. 1 is executed for the number of possible voltage vector states shown in Table. I for the inverter, in this case 9 vectors are obtained including 6 active states, 2 null states and 1 equivalent shoot through state. The prediction of the variable is done for each possible voltage vector state between two switching instants and the cost function (13) is calculated for each voltage vector. The voltage vector generating minimum value of $g^{\gamma}_{\delta\zeta}$ is applied to the inverter. There is no analytical approach to finding the weighing factors which are usually done empirically [39]. The previous systems proposed in literature generally employ more than 3 weighting factors which can make the tuning a complex task hence this problem is eliminated in the presented control. The tuning of factors is done in a way to ensure the stability of the system. Giving the preference to i_{L1} over $i_{\alpha\beta}$ as i_{L1} is the deciding factor for $i_{\alpha\beta}$ and if the change in $i_{\alpha\beta}$ is done faster than the i_{L1}, it can lead to stability issues of the V_{C1} due to extra demand of current on AC side. Also, rather than treating i_{α} and i_{β} as two different cost functions as in conventional MPC for grid-tied inverters [41, 42], in this paper, the proposed controller used the complex notation of the variable.

TABLE II: COST FUNCTION PARAMETERS

n	$\mathbf{I_{ref}}^{n}(\mathbf{k})$	$\mathbf{I}^{n}(\mathbf{k+1})$
1	$i^{\delta}_{L1ref}(k)$	$i_{L1}(k+1)$
2	$i^{\zeta}_{\alpha\beta ref}(k)$	$i_{\alpha\beta}(k+1)$

F. Lyapunov Stability Analysis of the System

System stability is analyzed using Lyapunov stability criterion. The future actual votage vector $v^{\alpha\beta,opt}_{qZSI}(k+1)$ required for perfect tracking can be represented as:

$$v^{\alpha\beta}_{qZSI}(k+1) = v^{\alpha\beta,opt}_{qZSI}(k+1) + \phi(k+1) \tag{14}$$

where, $v^{\alpha\beta}_{qZSI}(k+1)$ shows the converter output voltage vector based on 9 switching states, $v^{\alpha\beta,opt}_{qZSI}(k+1)$ is the optimum voltage vector that can make the current error in next sampling insatnt to zero and $\phi(k+1)$ represents the quantization error in the voltage vectors, here, $\left\|\phi(k+1)\right\| \le l$ and $l \in \mathbb{R}^{+}$.

Since, $v^{\alpha\beta}_{qZSI}(k+1)$ is bounded and is in finite sets, the hysteresis bounds of width $\phi(k+1)$ are also bounded, thus the existence of *'l'* is guaranteed. Taking control parameters defined above, $i_{\alpha\beta-error}$ can be defined as:

$$i_{\alpha\beta-error} = i_{\alpha\beta}(k+1) - i_{\alpha\beta-ref}(k+1) \tag{15}$$

From equation (6),

$$\begin{aligned} i_{\alpha\beta-error}(k+1) &= i_{\alpha\beta}(k)\left[1 - \frac{R}{L}T_S\right] \\ &+ \frac{T_S}{L}(v^{\alpha\beta}_{qZSI}(k) - e_{\alpha\beta}(k)) - i_{\alpha\beta-ref}(k+1) \end{aligned} \tag{16}$$

The goal of the control function is to reduce tracking error $i_{\alpha\beta-error}$ asymptotically to zero or a very small error tolerance value ε. The lyuponav function $L(k)$ is defined as:

$$L(i_{\alpha\beta-error}) = \frac{1}{2}\left[i_{\alpha\beta-error}(k)\right]^{T}\left[i_{\alpha\beta-error}(k)\right] \tag{17}$$

Using (16), the rate of change of lyuponav function can be defined as:

$$\begin{aligned} &\Delta L(i_{\alpha\beta-error}) = L(i_{\alpha\beta-error}(k+1)) - L(i_{\alpha\beta-error}(k)) \\ &\Delta L(i_{\alpha\beta-error}) = \\ &\frac{1}{2}\left[i_{\alpha\beta}(k)\left[1 - \frac{R}{L}T_S\right] + \frac{T_S}{L}(v^{\alpha\beta}_{qZSI}(k) + \phi(k+1) - e_{\alpha\beta}(k)) - i_{\alpha\beta-ref}(k+1)\right]^{T} \\ &\left[i_{\alpha\beta}(k)\left[1 - \frac{R}{L}T_S\right] + \frac{T_S}{L}(v^{\alpha\beta}_{qZSI}(k) + \phi(k+1) - e_{\alpha\beta}(k)) - i_{\alpha\beta-ref}(k+1)\right] \\ &-\frac{1}{2}\left[i_{\alpha\beta-error}(k)\right]^{T}\left[i_{\alpha\beta-error}(k)\right] \end{aligned} \tag{18}$$

This article has been accepted for publication in a future issue of this journal, but has not been fully edited. Content may change prior to final publication. Citation information: DOI 10.1109/JESTPE.2018.2823904, IEEE Journal of Emerging and Selected Topics in Power Electronics

According to lyuponav theorem, for convergence of $i_{\alpha\beta-error}$ to zero and for system to be stable, the rate of change of lyuponav function $\Delta L(i_{\alpha\beta-error})$ should be always negative, thus, $i_{\alpha\beta-error} \to 0$, $iff\ \Delta L(i_{\alpha\beta-error}) < 0$. The discrete future voltage vector which ensure the negative rate of change of $\Delta L(i_{\alpha\beta-error})$ is given by:

$$v_{qZSI}^{\alpha\beta} = \frac{L}{T_S} i_{\alpha\beta}(k+1) + i_{\alpha\beta}(k)\left[R - \frac{L}{T_S}\right] + e_{\alpha\beta} \tag{19}$$

For lyuponav stability, system should follow the following criteria:

$$\begin{aligned} &L(i_{\alpha\beta-error}(k)) \geq C_1 \left|i_{\alpha\beta-error}(k)\right|^{\sigma}, \forall i_{\alpha\beta-error}(k) \in \Upsilon \\ &L(i_{\alpha\beta-error}(k)) \geq C_2 \left|i_{\alpha\beta-error}(k)\right|^{\sigma}, \forall i_{\alpha\beta-error}(k) \in \Gamma \\ &L(i_{\alpha\beta-error}(k+1)) - L(i_{\alpha\beta-error}(k)) < -C_3 \left|i_{\alpha\beta-error}(k)\right|^{\sigma} + C_4 \\ &C_1, C_2, C_3, C_4 \in \mathbb{R}^+, \sigma \geq 1 \\ &\Upsilon \in \mathbb{R}^+, \Gamma \subset \Upsilon \end{aligned} \tag{20}$$

Substituting (19) in (18)

$$\Delta L(k) \leq \frac{1}{2}\left(\frac{T_S}{L}\right)^2 l^2 - \frac{1}{2}\left[i_{\alpha\beta-error}(k)\right]^T \left[i_{\alpha\beta-error}(k)\right] \tag{21}$$

Also, the current vector converges to compact given by equation (22)

$$\Omega = \left\{ \left\| i_{\alpha\beta-error}(k) \right\| \left\| i_{\alpha\beta-error}(k) \right\| \leq \frac{T_S}{L} l \right\} \tag{22}$$

From (20),

$$C_1 = C_2 = 1$$

$$C_3 = \frac{1}{2}, C_4 = \frac{1}{2}\left(\frac{L}{T_s}\right)^2 l^2$$

Therefore, all the signals will be bounded and will satisfy the Lyapunov stability criterion.

IV. Results and Discussions

The proposed system and controller is verified experimentally using dSPACE-DS1007 platform. The performance of the proposed PEI is evaluated for the following criteria: solar irradiance variation and reactive power compensation of the passive load connected at the PCC. The system is analyzed independently at the PV side for its MPP tracking performance by the system while simultaneously controlling the reactive power injection into the grid and their dynamic response on controlled parameters. Table. III shows the parameters of the system and Table. IV shows the controller parameters. The results are verified for above criteria and are shown in Fig. 5-Fig. 12. This section has been further divided for a clear overview as, A) PV side dynamics, B) Grid side dynamics, C) Parameter variation effect, and D) Proposed controller performance comparison.

TABLE III: System Parameters

Parameters	Values
V_{abc}	208VRMS (L-L)
Frequency	60Hz
PV MPP @ STC	2250W
V_{MP}	276.3V
I_{MP}	8.15A
RL Filter	1.5mH-0.01Ω
L1and L2	1mH
C1 and C2	1000μF

TABLE IV: Controller Parameters

Parameters	Values
Weight Factor i_{L1}	1
Weight Factor $i\alpha\beta$	0.25
Weight Factor for *fs*	0.02
Sampling Time (T_s)	100kHz
Average Switching frequency	22kHz

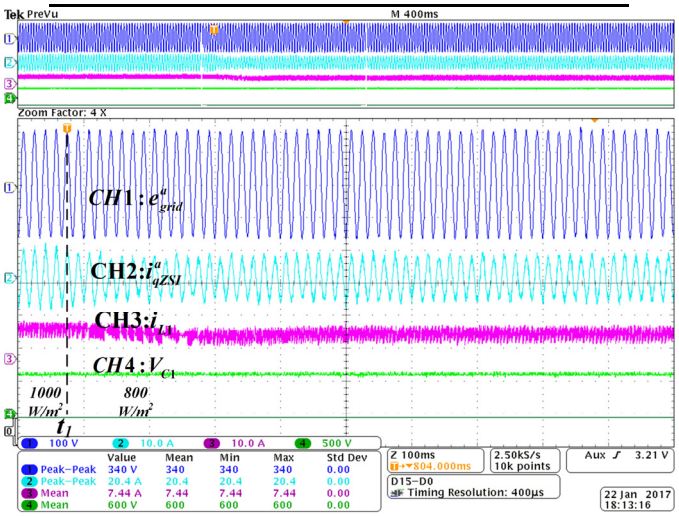

Fig. 5 The solar insolation changes from 1000W/m² to 800W/m². The step change in active power reference from the MPPT algorithm occurs at t_1. e^a_{grid} is the PCC voltage, i^a_{qZSI} is the phase a current fed by qZSI to PCC, il_1 is the qZSI input inductor current, and Vc1 is the qZSI C1 voltage.

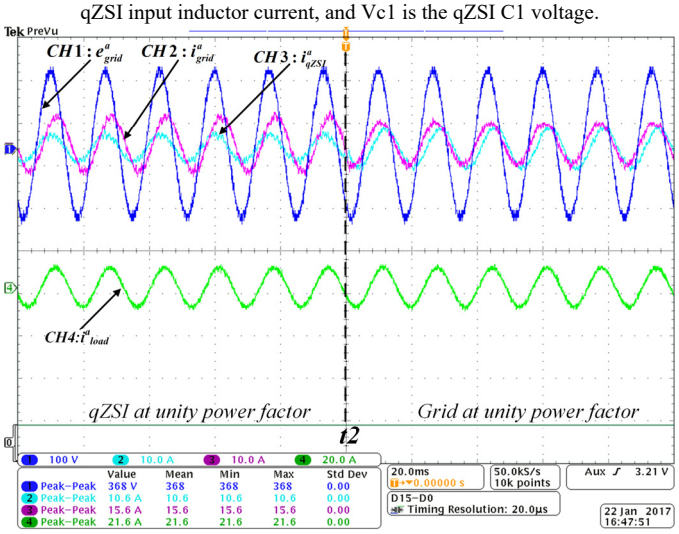

Fig. 6 Reactive power compensation by qZSI: grid current, grid voltage, inductive load current, and qZSI current waveforms before and after triggering the reactive power compensation.

This article has been accepted for publication in a future issue of this journal, but has not been fully edited. Content may change prior to final publication. Citation information: DOI 10.1109/JESTPE.2018.2823904, IEEE Journal of Emerging and Selected Topics in Power Electronics

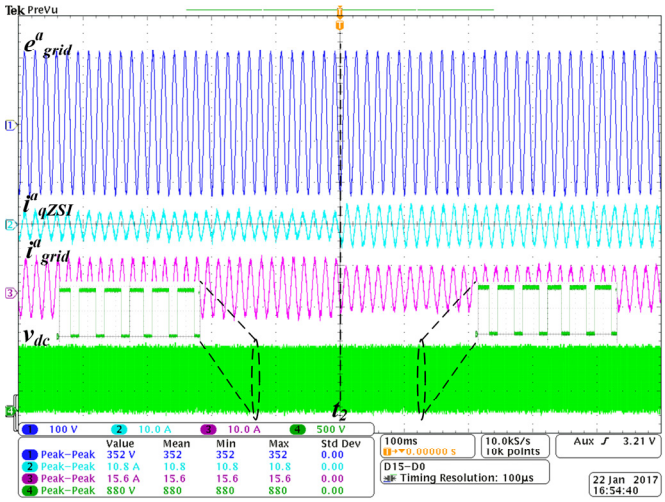

Fig. 7 Effect of triggering the reactive power compensation at t_2 by qZSI on DC-link voltage, grid current, and qZSI current. e^a_{grid} is the PCC voltage, i^a_{qZSI} is the phase a current fed by qZSI to PCC, i^a_{grid} is the grid current, and v_{dc} is the qZSI DC link pulsating voltage demonstrating boosting operation.

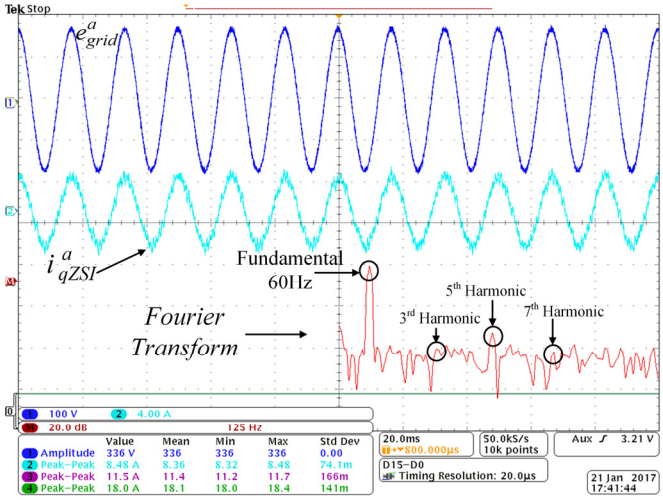

Fig. 8 Injected qZSI current and its FFT analysis.

A. PV Side dynamics

Fig. 5 shows the DC side parameters of the qZSI during the transient operation of the system. A step change is applied to solar irradiance level decreasing the irradiance from 1000W/m2 to 800W/m2, which is followed by the fall in i_{L1} as shown in Fig. 5. The V_{C1} was constantly maintained at 600V during the transient operation showing the dynamic performance and effectiveness of the control. The e_a and i_a are shown to be in-phase showing the active power injection by the qZSI. In this, qZSI is only catering the active power of the load by pushing the maximum available power from the PV.

B. Grid Side dynamics

Fig. 6 shows the reactive power compensation for the local loads shown in Fig. 1. The system is commanded to change the operation from lagging power factor to unity power factor at grid side by compensating the reactive power of the load by qZSI. During this time, qZSI will partially behave as STACOM. This paper adopts conventional load reactive power compensation method to show the effectiveness of the control. In Fig. 6, before instant t_2, the reactive power command was 0, thus all the reactive power is supplied by the grid and can be

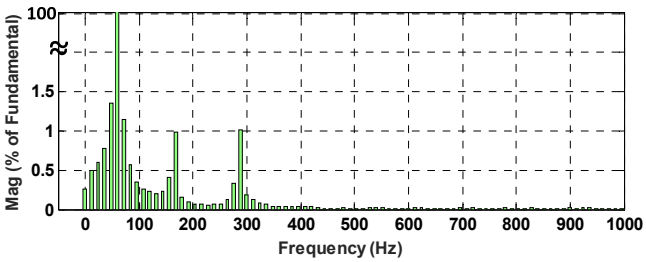

FIG. 9 Detailed FFT analysis

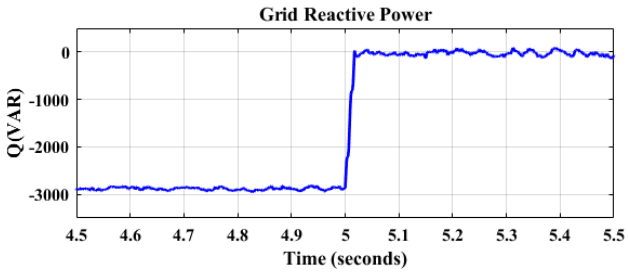

Fig. 10 Dynamic response of the grid reactive power to reactive power compensation by the qZSI.

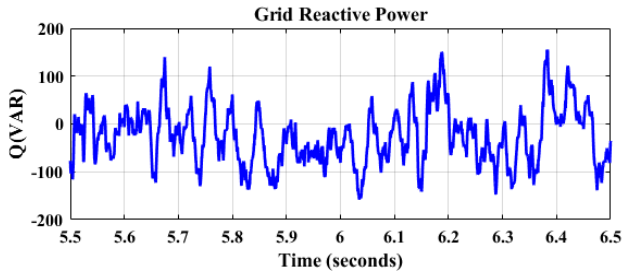

Fig. 11 Grid reactive power ripple after compensation by qZSI.

seen as grid current is leading the voltage and qZSI is operating at the unity power factor. At instant t_2, the reactive power is commanded to make the grid at unity power factor as in conventional STATCOMs, thus making grid at unity power factor and qZSI at leading. The reactive power demand of 750VAR has been compensated by the qZSI along with the PV MPP of 2.25kW.

Fig. 7 shows the DC link of qZSI, grid voltage, qZSI injected current and grid current for reactive power compensation, which was elaborated in Fig. 6. The pulsating DC link shows the boosting operation. The system followed the command without any DC link voltage spike. This ensures the system dynamic performance as well as current bound limits of the system. Current is limited within bounds eliminating the sudden spikes in the voltages which can result in damaging of semi-conductor devices. Also, the zoomed in DC link voltage before and after the reactive power commend verifies that the control maintains the same boosting ratio confirming that the system is maintaining MPP tracking independent of the reactive power injection. Fig. 8 shows the Fast Fourier Transform (FFT) of the injected qZSI currents. As seen, the system has high fundamental peak with all the harmonics distributed over the band. This is due to the variable switching frequency of the MPC. This is advantageous as the distribution of harmonics reduced the individual 3rd, 5th and 7th harmonic magnitude and provide low (3.2%) Total Harmonics Distortion (THD) current, which is within IEEE-519 standards [43]. The detailed FFT

This article has been accepted for publication in a future issue of this journal, but has not been fully edited. Content may change prior to final publication. Citation information: DOI 10.1109/JESTPE.2018.2823904, IEEE Journal of Emerging and Selected Topics in Power Electronics

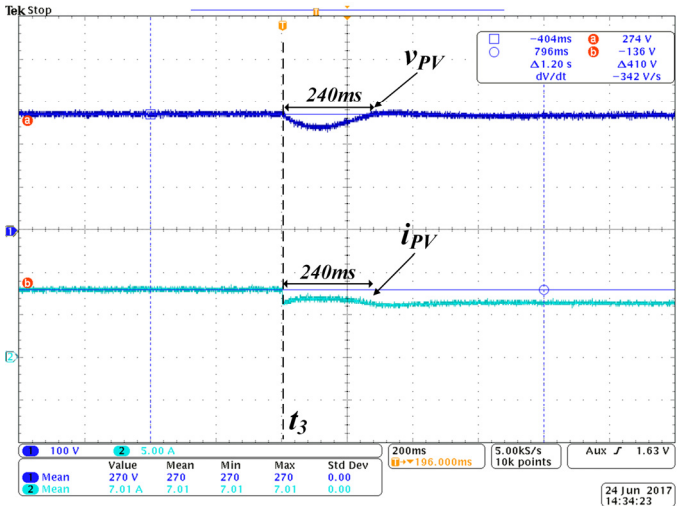

Fig. 12 Irradiance step change at t_3 from 1000W/m^2 to 800W/m^2.

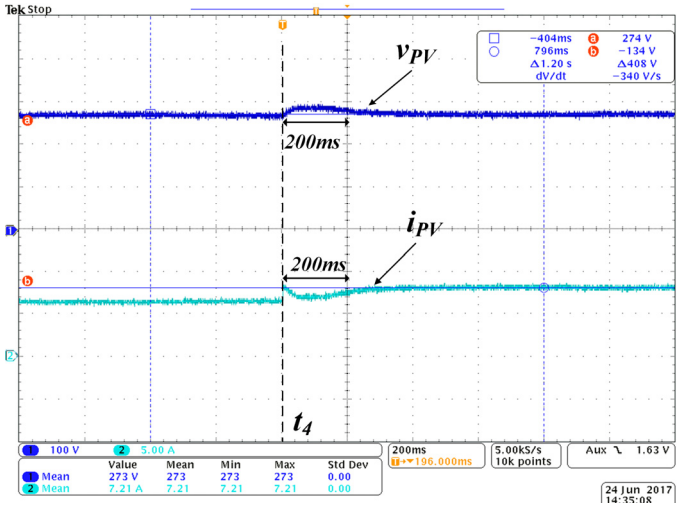

Fig. 13 Irradiance step change at t_4 from 800W/m^2 to 1000W/m^2.

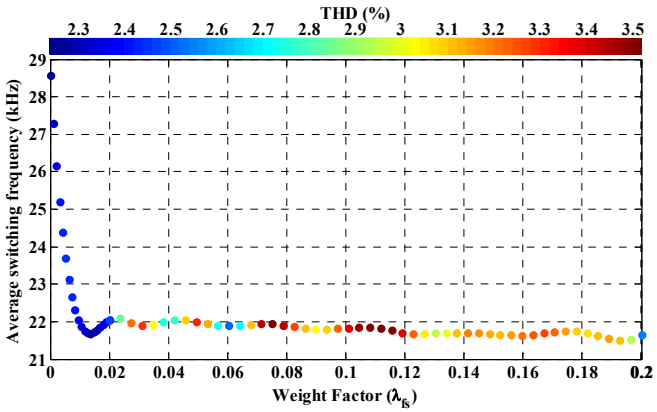

Fig. 14 Variation of switching frequency and THD with respect to weight factor of g_{fs}^{γ}.

TABLE V: PV MPP EFFICIENCY

IRRADIANCE (W/m^2)	PV MPP TRACKING EFFICIENCY (%)	RIPPLE (%)
1000	99.14	0.632
900	98.11	0.3735
800	98.165	0.6735

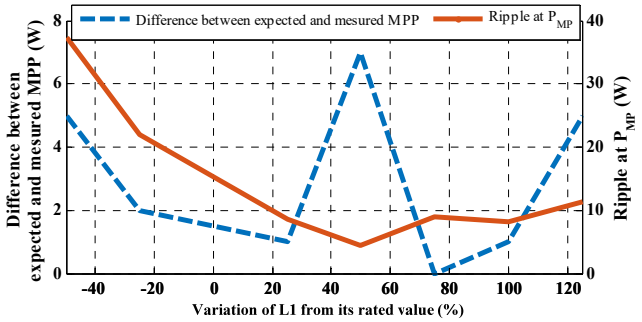

Fig. 15 Variation of L1 from its nominal model and its effect on MPP tracking at irradiance of 1000W/m^2.

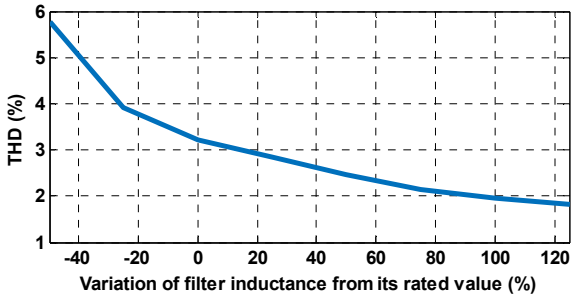

Fig. 16 Variation of filter inductance from its nominal model and its effect on THD at irradiance of 1000W/m^2.

waveform is shown in Fig. 9 to confirm the low THD of 3.2% which can be verified by looking at the harmonics percentages.

Fig. 10 shows the response of the grid to the reactive power compensation by the qZSI triggered at t=5sec and Fig. 11 shows the grid reactive power ripple and tracking error in steady state. Fig. 10 shows the fast-dynamic response of the system to the commanded reactive power and reach the steady state in less than 20ms, which is nearly one AC cycle of the grid. Fig.12 and Fig. 13 shows the performance of the MPPT and the current controller on V_{PV} and I_{PV} during positive (800W/m^2 to 1000W/m^2) and negative (1000W/m^2 to 800W/m^2) irradiance transients.

It can be seen from both the Fig. 12 and Fig. 13, that the PV voltage remains almost constant whereas the PV current has changed to track the MPP. The above-mentioned figures also demonstrate the speed at which the MPP is being tracked. During negative transient at t_3, Fig. 12, the sudden power decrease leads to voltage dip (undershoot) at the DC bus of around 80V. After the transient, the system recovered within 240ms and reached the previous voltage value as well as new MPP current of 6.15A with the MPP efficacy of 98.165%. During positive step at t_4 in Fig. 13, the overshoot is around 20V which is significantly lower than the undershoot as expected because at this point the extracted power is less than PV MPP. Therefore, system recovered in 200ms to the new MPP with the MPP current as 8.1A tracking MPP with an efficacy of 99.14%.

C. *Parameter Variations effect*

Fig. 14 shows the effect of optimal control effort on the system parameters like average switching frequency and THD of the injected current. The graph shows the variation of average switching frequency with weight factor λ_{fs}. The THD is represented by the color variation on the scattered points. The THD of the injected current is low at high switching frequency

This article has been accepted for publication in a future issue of this journal, but has not been fully edited. Content may change prior to final publication. Citation information: DOI 10.1109/JESTPE.2018.2823904, IEEE Journal of Emerging and Selected Topics in Power Electronics

as expected for low weight factors. The increase in weight factor decrease the frequency significantly in started showing the effect of the optimal control effort for minimizing the energy-losses per switching event.

Table. V Shows the MPP tracking efficiency of the system for various irradiance values and the corresponding power ripple. The overall system efficiency was found to be 85.6% at STC condition. The system maintained a good tracking accuracy and negligible power ripple of less than 1% for every irradiance. On the scale of 2.25kW, the power ripple is negligible and doesn't effect the system. In addition to test the MPC robustness with the parameter variation, both the parameters used in MPC are varied without changing the MPC algorithm and their corresponding affect on controller perfromance on MPP tracking, MPP ripple and maintaining low THD is analyzed. Fig. 15 and Fig. 16 shows the variation of input inductor L1 and filter inductor L variation respectively.

Fig. 15 shows the variation of L1 from -50% to 125% its rated value, and the PV MPP efficiency along with PV MPP ripples is measured. It is found that, the difference between the expected MPP and the measured is less than 8W for the whole L1 variation range which is 0.35% of the rated L1 MPP value. Further, the ripple at any variation point is within 2% of the maximum power at STC. Fig. 16 shows the same variation of filter inductance from -50% to 125% of its rated value and its affect on the THD value of the injected current. The THD value is in compliance and is 5.7% for the -50% variation in inductance.

The above analysis confirms the robustness of the controller on the model parameter variation of the system. Also, the effect of V_{C1} on the system will be negligible, as it is not included in the MPC algorithm to compute future values which require exact values. This is another advantage of using PI controller for the V_{C1} which automatically compensate for the variation of C1 and have negligible effect on the performance of the system.

D. Proposed Controller Dynamic Performance Analysis and Comparison

Fig. 17 shows the imported oscilloscope data of measured PCC voltage along with the grid current to clearly demonstrate the reactive power compensation and unity power factor operation. At t2, reactive power compensation is turned off as marked on Fig. 17. Lines have been marked before and after t2 to show the out of phase and in phase nature of the current to further verify the unity power operation after t2. Also, settling time has been marked showing the controller response time of less than one power cycle to achieve the compensation. The fast response shows the effectiveness of proposed control scheme.

Fig. 18 and Fig. 19 shows the tracking performance of active and reactive power for the experiment of Fig. 6 at time t2. Fig. 18 shows the tracking performance of the reactive power compensation. Reactive power compensation was triggered at 0.5sec. The system followed the reference and was able to track the reference under 250ms as can be verified from the Fig. 18. Similarly, Fig. 19 shows the tracking performance of the active power reference for the experiment of Fig. 5 at time t1 in the revised manuscript. For this, PV irradiance have been stepped to decrease the active power input to the system

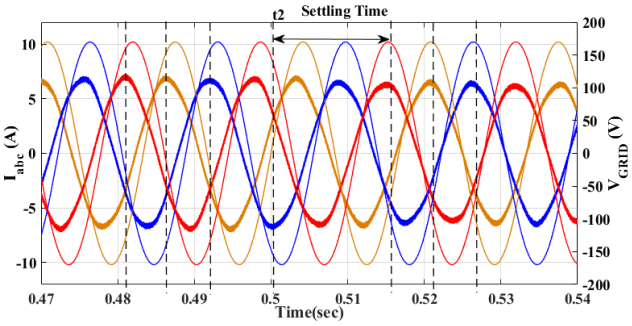

Fig. 17 Dynamic response of the grid reactive power to reactive power compensation by the qZSI.

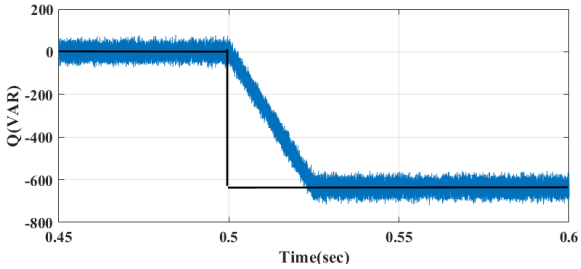

Fig. 18 Step response of reactive power compensation

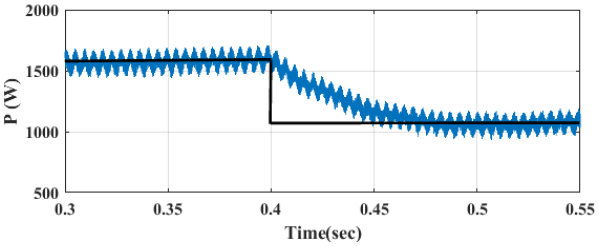

Fig. 19 Step response of active power compensation

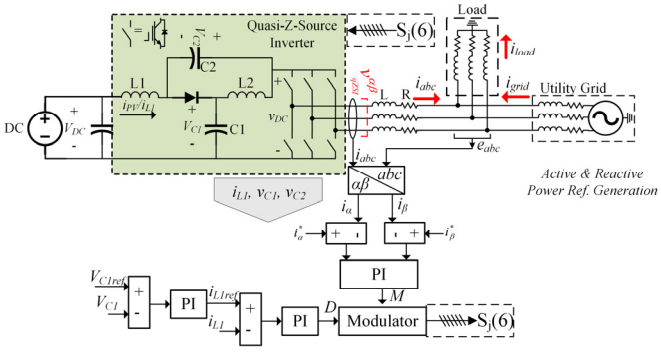

Fig. 20 Classical PI controller approach for the qZSI under study.

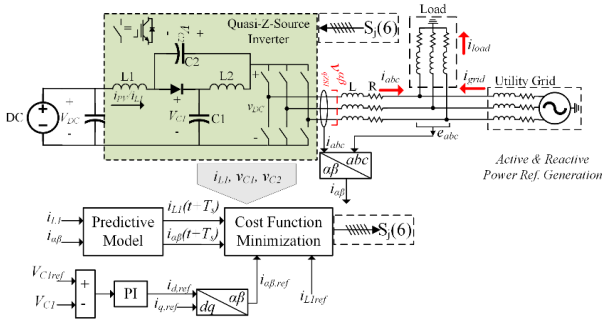

Fig. 21 The proposed control scheme based on MPC for qZSI with advance functionality.

which is followed by the MPPT and MPC controller which consequently reduce the active power injection into the grid. Further the performance comparison between classical

This article has been accepted for publication in a future issue of this journal, but has not been fully edited. Content may change prior to final publication. Citation information: DOI 10.1109/JESTPE.2018.2823904, IEEE Journal of Emerging and Selected Topics in Power Electronics

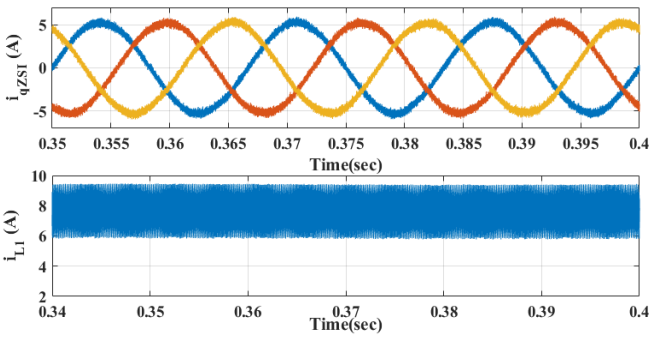

Fig. 22 Classical control-based response.

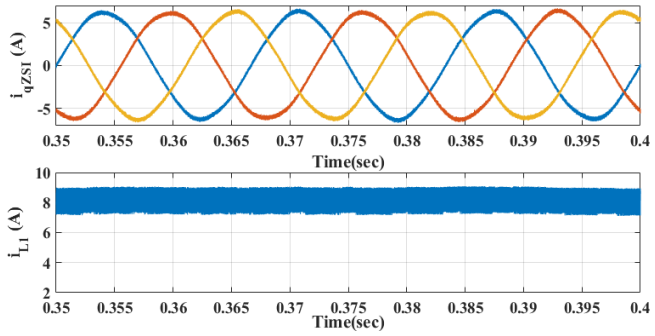

Fig. 23 MPC based control response.

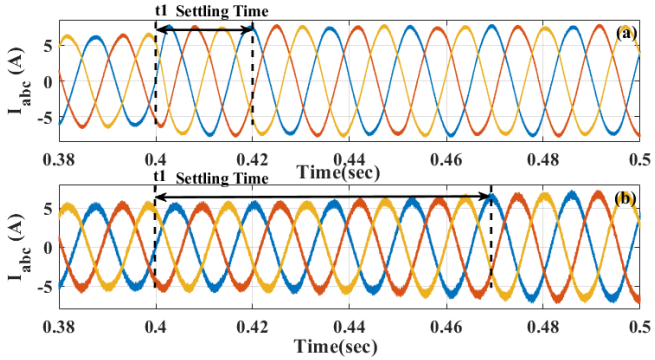

Fig. 24 (a) MPC, (b) classical based control response to step change in reactive power compensation.

controller and propose MPC based controller is performed. Fig. 20 shows the general classical controller and Fig. 21 shows the control block diagram of the proposed controller. In this analysis, the PI controller gains for conventional method are designed using the well-known Ziegler-Nichols method which is basically evaluates the step response of the system for determination of the gains, this technique is widely used in industry.

The structure of the proposed model based predictive controller differs from the PI based controller since there is no modulator and no cascaded liner controller which are challenging to tune and are not robust to grid abnormalities for the application in this paper. In the proposed system a single cost function is utilized for optimal actuation. Thus, it is easier to design since there are no cascaded modules as in classical linear controllers that must be tuned simultaneously to achieve smooth dynamic response and negligible active and reactive power tracking error in steady state operation.

Fig. 22 shows the output current and input inductor current using classical controller and Fig. 23 shows the same parameters using the MPC based controller. As can be observed the proposed controller has lower current ripple at both AC side and DC side input inductor. This is since MPC is hysteresis type of controller and can instantaneously follow the reference by applying the appropriate voltage vectors and thus, can achieve very small current ripples. Further, both the system has been compared for the step response for the reactive power compensation at t1. Fig. 24 shows the response comparison. Fig. 24 (a) shows the MPC response and Fig. 24(b) shows the classical control response. As can be observed, the MPC was able to respond within single cycle to achieve the reference whereas classical control took around 2-3 cycles.

V. Conclusion

A grid-tied PEI using qZSI for PV applications is developed based on MPC framework. The system is analyzed for PV application as Distributed Generation unit along with ancillary service requirement by the grid at PCC. The proposed control accurately generates the references of the variables to be controlled. A PI module is used to regulate the DC bus voltage and the conventional Incremental & Conductance algorithm for PV MPP current (I_{MP}) generation reference. Finally, the qZSI predictive model is used to generate the voltage vector and switching pulses for the qZSI leading to the lowest error between the predictive and reference values. The system also tackles the problem of overcurrent during grid faults and provide cycle by cycle overcurrent protection which is constraint to optimize the cost function. Further, a minimum energy controller is also included in the algorithm to minimize the switching effort to go from one voltage vector to another, thus, aims on reducing the switching losses. The system was first designed, simulated, and finally tested experimentally using dSpace-1007. The system was capable of tracking and delivering maximum power from PV with fast tracking dynamics along with independent reactive power compensation for the load/grid connected at the PCC. The system could condition the grid by supplying the required reactive power thus making grid operate at unity power factor.

References

[1] Z. Moradi-Shahrbabak, A. Tabesh, and G. R. Yousefi, "Economical Design of Utility-Scale Photovoltaic Power Plants With Optimum Availability," *IEEE Trans. on Ind. Elect.,* vol. 61, pp. 3399-3406, 2014.

[2] H. Long, M. Eghlimi, and Z. Zhang, "Configuration Optimization and Analysis of a Large Scale PV/Wind System," *IEEE Trans. on Sust. Energy,* vol. 8, pp. 84-93, 2017.

[3] S. B. Kjaer, J. K. Pedersen, and F. Blaabjerg, "A review of single-phase grid-connected inverters for photovoltaic modules," *IEEE Trans. on Ind. App.,* vol. 41, pp. 1292-1306, 2005.

[4] Y. Liu, B. Ge, H. Abu-Rub, and F. Z. Peng, "Control System Design of Battery-Assisted Quasi-Z-Source Inverter for Grid-Tie Photovoltaic Power Generation," *IEEE Trans. on Sust. Energy,* vol. 4, pp. 994-1001, 2013.

[5] M. Shen, A. Joseph, J. Wang, F. Z. Peng, and D. J. Adams, "Comparison of Traditional Inverters and Z -Source Inverter for Fuel Cell Vehicles," *IEEE Trans. on Pow. Elect.,* vol. 22, pp. 1453-1463, 2007.

[6] P. Fang Zheng, "Z-source inverter," *IEEE Trans. on Ind. App.,* vol. 39, pp. 504-510, 2003.

[7] Y. Li, S. Jiang, J. G. Cintron-Rivera, and F. Z. Peng, "Modeling and Control of Quasi-Z-Source Inverter for Distributed Generation Applications," *IEEE Trans. on Ind. Elect.,* vol. 60, pp. 1532-1541, 2013.

[8] D. Sun, B. Ge, W. Liang, H. Abu-Rub, and F. Z. Peng, "An Energy Stored Quasi-Z-Source Cascade Multilevel Inverter-Based Photovoltaic Power

Generation System," *IEEE Trans. on Ind. Elect.,* vol. 62, pp. 5458-5467, 2015.
[9] B. Anvari, M. Shirinabadi, and E. Afjei, "Design and Simulation of Z-Source Inverter for Brushless DC Motor Drive," *International Research Journal of Applied and Basic Sciences,* vol. 7, pp. 417-421, 2013.
[10] D. Cao, S. Jiang, X. Yu, and F. Z. Peng, "Low-cost semi-Z-source inverter for single-phase photovoltaic systems," *IEEE Transactions on Power Electronics,* vol. 26, pp. 3514-3523, 2011.
[11] A. Ayad, P. Karamanakos, and R. Kennel, "Direct Model Predictive Current Control Strategy of Quasi-Z-Source Inverters," *IEEE Trans. on Pow. Elect.,* vol. PP, pp. 1-1, 2016.
[12] D. Hamza, M. Qiu, and P. K. Jain, "Application and Stability Analysis of a Novel Digital Active EMI Filter Used in a Grid-Tied PV Microinverter Module," *IEEE Trans. on Pow. Elect.,* vol. 28, pp. 2867-2874, 2013.
[13] A. Abdelhakim, P. Davari, F. Blaabjerg, and P. Mattavelli, "Switching Loss Reduction in the Three-Phase Quasi-Z-Source Inverters Utilizing Modified Space Vector Modulation Strategies," *IEEE Transactions on Power Electronics,* 2017.
[14] V. Erginer and M. H. Sarul, "A novel reduced leakage current modulation technique for Z-source inverter used in photovoltaic systems," *IET Power Electronics,* vol. 7, pp. 496-502, 2013.
[15] N. Noroozi and M. R. Zolghadri, "Three-Phase Quasi-Z-Source Inverter with Constant Common-Mode Voltage for Photovoltaic Application," *IEEE Transactions on Industrial Electronics,* 2017.
[16] Y. Zhou, L. Liu, and H. Li, "A high-performance photovoltaic module-integrated converter (MIC) based on cascaded quasi-Z-source inverters (qZSI) using eGaN FETs," *IEEE Transactions on Power Electronics,* vol. 28, pp. 2727-2738, 2013.
[17] J. Anderson and F. Z. Peng, "Four quasi-Z-Source inverters," in *2008 IEEE Power Electronics Specialists Conference*, 2008, pp. 2743-2749.
[18] A. Anurag, Y. Yang, and F. Blaabjerg, "Thermal performance and reliability analysis of single-phase PV inverters with reactive power injection outside feed-in operating hours," *IEEE Journal of emerging and selected topics in power electronics,* vol. 3, pp. 870-880, 2015.
[19] A. Hoke, M. Shirazi, S. Chakraborty, E. Muljadi, and D. Maksimovic, "Rapid Active Power Control of Photovoltaic Systems for Grid Frequency Support," *IEEE Journal of Emerging and Selected Topics in Power Electronics,* 2017.
[20] Y. Yang, H. Wang, and F. Blaabjerg, "Reactive Power Injection Strategies for Single-Phase Photovoltaic Systems Considering Grid Requirements," *IEEE Transactions on Industry Applications,* vol. 50, pp. 4065-4076, 2014.
[21] F. Cleveland, "Recommendations for Advanced Functions for Distributed Energy Resources (DER) Systems," March 12, 2015 ed. California: Public Utilities Commision, 2015, pp. 1-12.
[22] P. Cortes, M. P. Kazmierkowski, R. M. Kennel, D. E. Quevedo, and J. Rodriguez, "Predictive Control in Power Electronics and Drives," *IEEE Trans. on Ind. Elect.,* vol. 55, pp. 4312-4324, 2008.
[23] N. Panten, N. Hoffmann, and F. W. Fuchs, "Finite control set model predictive current control for grid-connected voltage-source converters with LCL filters: A study based on different state feedbacks," *IEEE Transactions on Power Electronics,* vol. 31, pp. 5189-5200, 2016.
[24] M. B. Shadmand, M. Mosa, R. S. Balog, and H. Abu-Rub, "Model Predictive Control of a Capacitorless Matrix Converter-Based STATCOM," *IEEE Journal of Emerging and Selected Topics in Power Electronics,* vol. 5, pp. 796-808, 2017.
[25] S. Vazquez, J. Rodriguez, M. Rivera, L. G. Franquelo, and M. Norambuena, "Model Predictive Control for Power Converters and Drives: Advances and Trends," *IEEE Trans. on Ind. Elect.,* vol. 64, pp. 935-947, 2017.
[26] L. Tarisciotti, A. Formentini, A. Gaeta, M. Degano, P. Zanchetta, R. Rabbeni*, et al.*, "Model Predictive Control for Shunt Active Filters With Fixed Switching Frequency," *IEEE Trans. on Ind. App.,* vol. 53, pp. 296-304, 2017.
[27] V. Yaramasu, B. Wu, M. Rivera, and J. Rodriguez, "A new power conversion system for megawatt PMSG wind turbines using four-level converters and a simple control scheme based on two-step model predictive strategy—Part II: Simulation and experimental analysis," *IEEE Journal of Emerging and Selected Topics in Power Electronics,* vol. 2, pp. 14-25, 2014.
[28] H. A. Hussain, B. Anvari, and H. A. Toliyat, "A control method for linear permanent magnet electric submersible pumps in a modified integrated drive-motor system," in *IEEE International Electric Machines and Drives Conference (IEMDC)*, 2017, pp. 1-7.
[29] D. M. Vilathgamuwa, C. J. Gajanayake, and P. C. Loh, "Modulation and control of three-phase paralleled Z-source inverters for distributed generation applications," *IEEE Transactions on energy conversion,* vol. 24, pp. 173-183, 2009.
[30] Y. Liu, B. Ge, H. Abu-Rub, H. Sun, F. Z. Peng, and Y. Xue, "Model Predictive Direct Power Control for Active Power Decoupled Single-Phase Quasi-Z-Source Inverter," *IEEE Trans. on Ind. Inform.,* vol. 12, pp. 1550-1559, 2016.
[31] W. Wu, Y. He, T. Tang, and F. Blaabjerg, "A New Design Method for the Passive Damped LCL and LLCL Filter-Based Single-Phase Grid-Tied Inverter," *IEEE Transactions on Industrial Electronics,* vol. 60, pp. 4339-4350, 2013.
[32] J. Xu, S. Xie, and T. Tang, "Active Damping-Based Control for Grid-Connected LCL-Filtered Inverter With Injected Grid Current Feedback Only," *IEEE Trans. on Ind. Elect.,* vol. 61, pp. 4746-4758, 2014.
[33] S. Jayalath and M. Hanif, "Generalized LCL-Filter Design Algorithm for Grid-Connected Voltage-Source Inverter," *IEEE Trans. on Ind. Elect.,* vol. 64, pp. 1905-1915, 2017.
[34] D. Pan, X. Ruan, C. Bao, W. Li, and X. Wang, "Optimized Controller Design for LCL-Type Grid-Connected Inverter to Achieve High Robustness Against Grid-Impedance Variation," *IEEE Trans. on Ind. Elect.,* vol. 62, pp. 1537-1547, 2015.
[35] J. Khajesalehi, K. Sheshyekani, M. Hamzeh, and E. Afjei, "High-performance hybrid photovoltaic -battery system based on quasi-Z-source inverter: application in microgrids," *IET Generation, Transmission & Distribution,* vol. 9, pp. 895-902, 2015.
[36] Y. Zhang, S. Huang, and S. Hu, "Ride-through strategy of quasi-Z-source wind power generation system under the asymmetrical grid voltage fault," *IET Electric Power Applications,* vol. 11, pp. 504-511, 2017.
[37] M. Mosa, R. Balog, and H. Abu-Rub, "High Performance Predictive Control of Quasi Impedance Source Inverter," *IEEE Trans. on Power Elect.,* vol. PP, pp. 1-1, 2017.
[38] K. S. Tey and S. Mekhilef, "Modified Incremental Conductance Algorithm for Photovoltaic System Under Partial Shading Conditions and Load Variation," *IEEE Trans. on Ind. Elect.,* vol. 61, pp. 5384-5392, 2014.
[39] S. Bayhan, M. Trabelsi, H. Abu-Rub, and M. Malinowski, "Finite Control Set Model Predictive Control for a Quasi-Z-Source Four-Leg Inverter Under Unbalanced Load Condition," *IEEE Trans. on Ind. Elect.,* vol. PP, pp. 1-1, 2016.
[40] M. Mirhosseini, J. Pou, and V. G. Agelidis, "Single- and Two-Stage Inverter-Based Grid-Connected Photovoltaic Power Plants With Ride-Through Capability Under Grid Faults," *IEEE Trans. on Sust. Energy,* vol. 6, pp. 1150-1159, 2015.
[41] S. Bayhan, H. Abu-Rub, and R. S. Balog, "Model Predictive Control of Quasi-Z-Source Four-Leg Inverter," *IEEE Trans. on Ind. Elect.,* vol. 63, pp. 4506-4516, 2016.
[42] S. Bayhan, M. Trabelsi, and H. Abu-Rub, "Model Predictive Control of Z-Source four-leg inverter for standalone Photovoltaic system with unbalanced load," in *2016 IEEE (APEC)*, 2016, pp. 3663-3668.
[43] I. W. Group, "IEEE recommended practices and requirements for harmonic control in electrical power systems," *IEEE STD,* pp. 519-1992, 1992.

Sarthak Jain (S'13) received the B.Tech. degree in electrical engineering from GGSIPU, Delhi, India, in 2014. He is currently working towards his master's degree in electrical engineering from Texas A&M University, College Station, TX, USA.

He was research associate in Renewable Energy and Advanced Power Electronics Laboratory from 2016-2017. Before joining Texas A&M University, he was research associate at Delhi Technological University, Delhi, INDIA from 2014-2016. There, he worked on a project titled 'Reliability and Efficient System for Community Energy Solutions (RESCUES)' under Imperial College London and DST INDIA. His research interest includes power electronics circuit design, DC/AC PV grid tied inverters, DC/DC resonant converters, etc.

This article has been accepted for publication in a future issue of this journal, but has not been fully edited. Content may change prior to final publication. Citation information: DOI 10.1109/JESTPE.2018.2823904, IEEE Journal of Emerging and Selected Topics in Power Electronics

Mohammad B. Shadmand (S'09, M'15) received the B.S. degree in electrical engineering from Qatar University, Doha, Qatar, in 2010. He received the M.S. and PhD degrees in electrical engineering from Texas A&M University, College Station, TX, USA in 2012 and 2015.

He was a research associate in renewable energy and advanced power electronics research laboratory, TX, USA from 2010-2015. He was a visiting researcher with Smart Grid Center, Texas A&M University at Qatar, 2014. He was an instructor in Department of Electrical and Computer Engineering, Texas A&M University, College Station, TX, USA from 2015-2016. He was a TEES research engineer in renewable energy and advanced power electronics research laboratory, TX, USA from 2016-2017. He is currently an Assistant Professor in the Department of Electrical and Computer Engineering and Director of the Renewable Energy and Power Quality Research Laboratory at Kansas State University, Manhattan, KS, USA since 2017. He has published more than 50 journal and conference papers. His current research interests include advanced model predictive control, grid-tied power electronics interfaces with advance functionalities, matrix converter, and control of smart microgrid systems.

Dr. Shadmand was awarded second place in the IEEE Industrial Application Society Graduate Thesis Contest for his M.S. thesis in 2013. He received the IEEE Standard Education award for the project "fixed-step model predictive control of grid-tied photovoltaic inverter" in 2014. He was awarded Michelle Munson_serban Simu Keystone Research Scholar, Kansas State University in 2017.

Robert S. Balog (S'92–M'96–SM'07) received the B.S. degree in electrical engineering from Rutgers – The State University of New Jersey, New Brunswick, NJ in 1996 and the M.S. and Ph.D. degrees in electrical engineering from the University of Illinois at Urbana-Champaign, Urbana, IL in 2003 and 2006 respectively.

He was an Engineer with Lutron Electronics, Coopersburg, PA from 1996 to 1999, a Researcher with the U.S. Army Corp of Engineers, Engineering Research and Development Center (ERDEC), Construction Engineering Research Lab (CERL), Champaign, IL from 2005-2006, a Senior Engineer at SolarBridge Technologies (now SunPower Inc.), Champaign, IL from 2006 to 2009, then joined Texas A&M University, College Station, Tx, where he is currently an Associate Professor in the Department of Electrical and Computer Engineering and Director of the Renewable Energy & Advanced Power Electronics Research Laboratory. He holds a joint faculty appointment with the Department of Electrical Engineering at Texas A&M University in Qatar.

He holds 18 issued U.S. patent with additional patents pending. His current research interests include power converters for solar energy, particularly microinverters for ac photovoltaic (ACPV) modules and highly reliable electrical power and energy systems including dc microgrids. Dr. Balog is a Registered Professional Engineer in Illinois. He received the IEEE Joseph J. Suozzi INTELEC Fellowship in Power Electronics in 2001. He is a member of Eta Kappa Nu, Sigma Xi, the National Society of Professional Engineers, the American Solar Energy Society and the Solar Electric Power Association. He is the 2011 recipient of the Rutgers School of Engineering Distinguished Engineer award.